

## Multi-scale Adaptive Dehazing Network

Shuxin Chen<sup>1</sup> Yizi Chen<sup>1</sup> Yanyun Qu<sup>1\*</sup> Jingying Huang<sup>1</sup> Ming Hong<sup>1</sup>

<sup>1</sup>Fujian Key Laboratory of Sensing and Computing for Smart City,  
School of Information Science and Engineering, Xiamen University, Fujian, China

2534641195@qq.com, atavism@msn.cn, yyqu@xmu.edu.cn, jyhuang33@outlook.com, 1184307675@qq.com

### Abstract

Since haze degrades an image including contrast decreasing and color lost, which has a negative effect on the subsequent object detection and recognition, single image dehazing is a challenging visual task. Most existing dehazing methods are not robust to uneven haze. In this paper, we developed an adaptive distillation network to solve the dehaze problem with non-uniform haze, which does not rely on the physical scattering model. The proposed model consists of two parts: an adaptive distillation module and a multi-scale enhancing module. The adaptive distillation block redistributes the channel feature response via adaptively weighting the input maps. And then the important feature maps are dissociated from the trivial for further focused learning. After that, a multi-scale enhancing module containing two pyramid downsampling blocks is employed to fuse the context features for haze-free images restoration in a coarse-to-fine way. Extensive experimental results on synthetic and real datasets demonstrates that the proposed approach outperforms the state-of-the-arts in both quantitative and qualitative evaluations.

### 1. Introduction

In poor weather conditions, the digital image will be degraded when it's photographed in the hazy scene, because the particles such as the haze and dusts interfere with the imaging process which results in the low contrast, color distortion and blurring problems. Because of this, dehazing which can improve the quality of hazy images is highly desired in photography, autonomous vehicles and other diversity computer vision applications [16].

Many successful dehazing methods are based on the physical scattering model [15] which is established by studying the scatter of light by atmospheric particles. The physical model is formulate as

$$I(z) = J(z)t(z) + A(z)(1 - t(z)), \quad (1)$$

\*Corresponding author

where  $I$  is the input hazy images,  $J$  is the restored images,  $t$  and  $A$  represent the medium transmission map and the global atmospheric light respectively. The restoration of clear images through the physical scattering model [15] depends on the estimation of transmission map and the atmospheric light. However, the estimation is an ill-posed task. Early methods utilizes various priors to settle the ill-posed problem so that the image can be restored. He et al. [8] proposed the theory of dark channel prior (DCP) for the prediction of transmission map. Zhu et al. [23] reconstructs transmission map based on the observation of color attenuation prior (CAP). While those prior-based methods are not robust enough in real-world scene. Recently, learning-based methods are more popular because of the rise of deep learning. Some of them use convolutional neural network (CNN) to estimate the parameter of the physical model and restore clear images. A common practice is to use deep neural networks to predict transmission maps from the hazy images [19] [2], there are also some networks designed to jointly predict the transmittance and the airlight [22] [21]. Since these methods are still limited to the dehazing model, when the parameters of the model are not accurately predicted, the removal performance is reduced. And for non-uniform weather conditions, they often fail to estimate the haze accurately, which in turn affects the subsequent dehazing.

In order to get over the parameter limitation brought by the physical model, we strive to achieve dehazing directly from the input hazy images to the scene radiance without drawing support from the physical model. Due to the existing methods face challenges in uneven haze and dense fog conditions, a solution which can autonomous focus on the learning of important features is required. The knowledge distillation network [10] which performs feature diversion according to the learned weights, and then strengthens learning on important features works. Based on this we introduce distillation in the dehazing. For the dehazing task, if we exact the haze-related knowledge from the input hazy maps and transfer them to a specific network for centralized learning, the dehazing performance of the entire model is

expected to elevate.

In this work, we introduce a Multi-scale Adaptive Dehazing Network (MADN) to complete the single image haze removal. Our network consists of two parts: an adaptive distillation module and a multi-scale enhancing module. The adaptive distillation module focuses on learning of the key knowledge. It autonomously learns the importance of the feature maps and separates the master feature maps from the secondary according to the learned feature weight and then carry out further information learning. Important features, embodying more information, plays a key role in the overall recovery. This part should be the back bone of our attention. While the other information plays a supporting role and contributes less to the whole model, correspondingly deserving less concern. The multi-scale enhancing module comply the comprehension learning in a coarse-to-fine way. By combining learning from local focus and global perspective, our network obtain more accurate and exhaustive learning. We perform our experiments on SOTS of RESIDE [13] and the NTIRE 2019 challenge on single image dehazing datasets Dense Haze [4].

The contributions of our work are summarized as follows:

1. We implement an adaptive distillation network for single image dehazing which redistributes channel response through an adaptive distillation module. So the useful and useless feature maps are adaptively separated by distillation and each carry out corresponding further learning.
2. We employ a multi-scale enhancing module which includes a pyramid pooling [11] block to fuse global and detail information to restore hazy image from coarse to fine.
3. We compare our proposed method with several representative state-of-the-art methods on both synthetic and real-world datasets. Our approach achieves superior performance in both visual effect and evaluation metrics.

## 2. Related Work

In this part, we mainly review the related methods which are used to address the single image dehazing task. The existing dehazing methods can be roughly categorized two classes: prior-based and learning-based.

**Prior-based approaches.** Early attempts focus on the extrinsic characteristics of images. Prior-based methods exploits statistical properties and hand-crafted features of natural images. Dark Channel Prior(DCP) [8], proposed by He, has made a hit then and used widely even now, which

presents its outstanding performance in the dehazing filed. However, the computational cost of soft matting which is used to smooth the transmission map has been suggested high. [6] presumes that in a small image patch, pixels satisfy a one-dimensional distribution of the RGB-space [18], based on color-lines assumption, the transmission map can be estimated. Berman et al. proposed non-local dehazing(NLD) [1] which indicates that a sharp image contains few hundreds of different colors. These colors cluster and appear in the form of haze line. The position of the pixel in the haze line is consistent with its attributes in the original image. prior-based methods exhibit excellent dehazing in the past few years, while the dependence on priors and assumptions makes them somewhat limited.

**Learning-based approaches.** Learning-based methods emerged following the trend of deep learning. Some of them based on the physical model predicts transmission maps and atmospheric light independent of physical priors. MSCNN [19] is one of the first to construct for single image dehazing, which learns the mapping between input hazy images and transmission maps. DehazeNet [2] proposes a novel network architecture and estimates the transmission map directly in an end-to-end manner given an input hazy image. AOD-Net [12] employs a multi-scale network to jointly estimate the transmittance and atmospheric light. Since it uses a unified representation, the haze-free image can be directly reconstructed, which reduces errors caused by two-step calculation. The arrival of Generative Adversarial Networks [7] has led a novel fashion for learning-based dehazing. Yan et.al. [14] combined the atmospheric scattering model with GAN, and DehazeGAN [22] applies GAN to generate both transmittance and air light. Besides, some model-free methods have recently appeared for single image dehazing. GFN [20] directly completes the generation of hazy maps to haze-free maps through a fusion-based strategy. It used a multi-scale structure, where the output of the coarse network is added to the fine network as input.

## 3. Proposed Method

### 3.1. Architecture

In this paper, we proposed a Multi-scale Adaptive Dehazing Network (MADN) to directly learn a mapping from the input hazy image to the clear image. The architecture of MADN is shown in Figure 1. It consists of two steps of adaptive distillation and multi-scale enhancement, with corresponding modules we call AD module and ME module. The AD module mainly contains three Adaptive Distillation blocks (AD block), while the ME module includes two enhancing blocks.

**Adaptive Distillation module.** Benefited from the distillation network [10], We utilities AD blocks to our dehazing network. The role of AD block is to elect the master

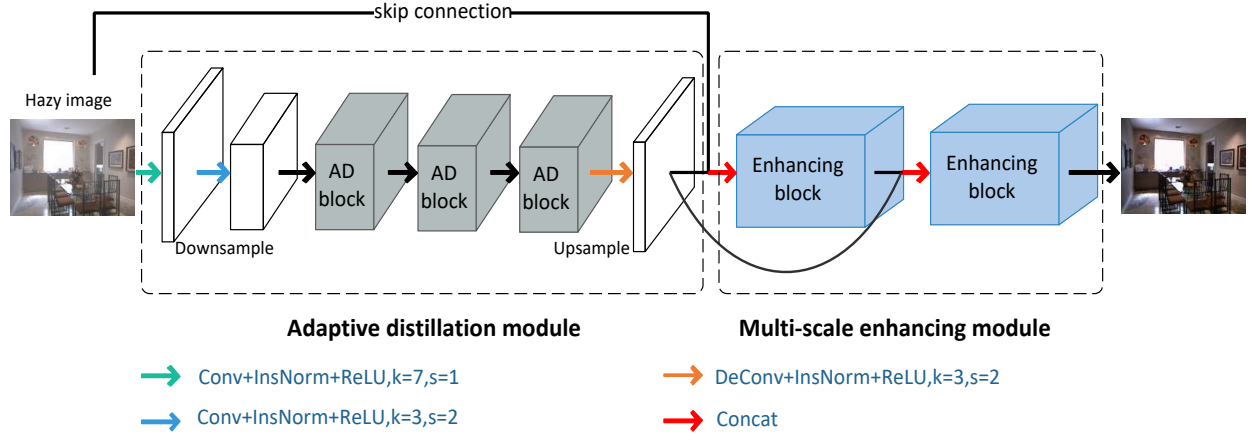


Figure 1. The Architecture of MADN.

feature maps from the secondary via corresponding weights and strengthen learning of important features. That is to say, feature maps passing through the block will be given a weight, according to which the separation of useful and useless feature maps will be performed. For important feature maps, the network automatically pay more attention to learning.

As shown in Figure 2, the input hazy image, first passes through three convolutions in the front of AD block, then a SE block [9] and a light SE (L-SE) are utilized to learn weights and threshold. Features with large weights learned next by three  $3 \times 3$  convolutions, and features with small weights learned by one  $1 \times 1$  convolution. The output of the two-way learning is added. SE consists of a global pooling layer, a full connection and a ReLU activation, followed by another full connection layer, a sigmoid function which achieves a linear transformation and finally output weights respectively for each feature map. L-SE block can be seen a streamlined SE with only a global pooling and a linear transformation layer embedded. The function of L-SE is to produce a threshold of our AD block. SE and L-SE act as shunts in this module which measures the weight of each feature in the input and assign high attention to areas with good weight and low values to ones with poor weight. Specially, when the weight of feature map is greater than the threshold, the feature map is transferred to the next convolution block for reinforce learning. The rest trivial features, united with input feature maps, eventually gathered with another well-learned feature branch.

**Multi-scale Enhancing module.** We introduce a Multi-scale Enhancing module (ME module) to strengthen the learning ability of the network. The ME module contains two enhancing blocks of which the architecture is shown in

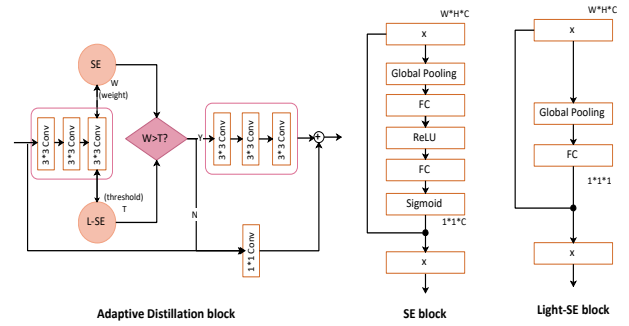


Figure 2. The structure of AD block, SE block and L-SE block.

Figure 3. The first is fed into the original image and the output from the front-end AD module. The result from the first enhancing block, concatenated with the output from AD module, serves as the input to the second enhancing block. This connection makes the flow of information both inherited and preserved. Feature maps, processed by two  $3 \times 3$  convolution kernels, is subjected to downsample according to the scale factors of 4, 8, 16, 32 respectively, and thus a four-scale pyramid pooling block [11] is formed. Each layer in the pyramid passes through a convolution layer with filter size  $1 \times 1$ , and upsample to primitive size. Feature maps before and after the pyramid pooling are concatenated together. At the end, we use a  $3 \times 3$  convolution for dimension alignment. By merging multi-scale features, our network is equivalent to learning knowledge based on different receptive field, and thus get finer feature representation ability via learning in both global and fine granularity.

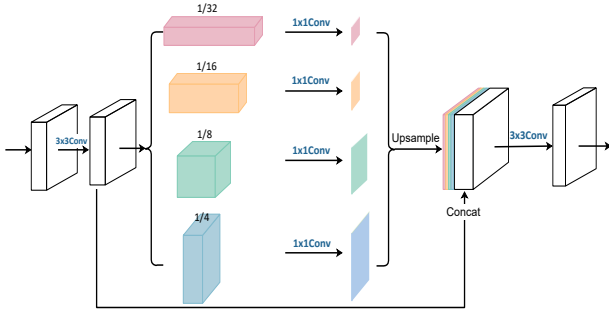


Figure 3. The architecture of enhancing block.

### 3.2. Loss function

We optimize the linear combination of the perceptual loss  $L_P$  and the similarity loss  $L_S$ .

**Perceptual loss.** We involves perceptual loss  $L_P$  to measure the high-level difference between the hazy and the corresponding target images. It is beneficial to improve semantic fidelity of the feature map. In this work,  $L_P$  is based on a pre-trained VGG-16 network [11] from which we draw the activations of the  $i$ -th layer as the perceptual feature we need. The aim is to minimize the difference between the perceptual features of the hazy and the ground truth image. We use the Euclidean distance as the measure criteria. The perceptual loss function is defined as

$$L_P = \frac{1}{C_i W_i H_i} \sum_{c=1}^{C_i} \sum_{x=1}^{W_i} \sum_{y=1}^{H_i} (\phi(\hat{I}_{c,x,y}) - \phi(J_{c,x,y}))^2 \quad (2)$$

where  $\hat{I}$  is the hazy image,  $J$  is the ground truth image.  $W_i$ ,  $H_i$ ,  $C_i$  indicate the width, the height and the channel of the  $i$ -th layer feature map.  $\phi$  is an operator of non-transformation that extracting a  $C_i \times W_i \times H_i$  feature map in VGG-16.  $(c, x, y)$  is the pixel position.

**Similarity loss.** In order to more accurately combine the information of the original image and improve the prediction, we measured the pixel-wise difference as the similarity loss. We compute the Euclidean distance between the hazy images and the counterpart images. The similarity loss is as follow

$$L_S = \frac{1}{CWH} \sum_{c=1}^C \sum_{x=1}^W \sum_{y=1}^H (\hat{I}_{c,x,y} - J_{c,x,y})^2 \quad (3)$$

where  $C$  is the channels of the original image,  $W$  and  $H$  denote the input size.  $\hat{I}$ ,  $J$  and  $(c, x, y)$  mean the same as before.

By combing the perceptual loss and similarity loss, our overall loss function is defined as

$$L = \lambda_1 L_P + \lambda_2 L_S \quad (4)$$

where  $(\lambda_1, \lambda_2)$  is the coefficient that control the weight of each term.

## 4. Experiments

In this section, we describe the datasets we used for training and testing along with some training details. We qualitatively and quantitatively evaluate the dehazing results of our proposed method with some other state-of-the-art methods.

### 4.1. Datasets

**RESIDE** [13]. As a standard benchmark widely used in dehazing task, RESIDE [13] consists of both indoor and outdoor, both synthetic and real-world hazy images. There are totally five subsets in it: Indoor Training Set (ITS), Synthetic Objective Testing Set (SOTS), Hybrid Subjective Testing Set (HSTS), Outdoor Training Set (OTS) and Real-world Task-driven Testing Set (RTTS). In our work, we use ITS which consists of 13990 synthetic images to train our network. SOTS is employed as our testing set, which includes 500 indoor and 500 outdoor images. In addition, we implement our method on some other real-world images used by previous methods for further evaluation.

**Dense Haze** [4]. The NTIRE2019 challenge dataset on single image dehazing which is named Dense Haze [4], contains 45 training data, 5 validation data and 5 test data. The hazy images are generated via professional devices in various indoor and outdoor environments. Their corresponding hazy-free images are collected in the same scenes. The resolution of all images is the same  $1600 \times 1200$ .

**I-HAZE** [17] & **O-HAZE** [3]. The NTIRE2018 dehazing challenge [5] datasets consist of two subsets: the indoor data (I-HAZE) and the outdoor data (O-HAZE), which involve 25 and 35 hazy images separately. The corresponding ground truth images are provided by the organizers as well. All the competition images with unequal high resolutions were collected using professional haze machines to ensure the hazy images and hazy-free images are captured in the same scene.

### 4.2. Experimental setting

**Data augmentation.** As for Dense Haze [4] dataset, to enrich the training set, we adopt measures to augment the 45 training images. In detail, the training set is divided into three parts according to the representative contents: wall, sky and others. For every part, we resize the images according to four distinctive proportions of the original size. At this time, four classes of images with various resolutions are obtained. The first class remains the same. Each image of the other three classes is cropped into 4, 16, 16 respectively. In addition, all images are flipped in four ways: keep as is, horizontally, vertically, horizontally and then vertically. After the above series of operations, we finally got 7236 training data.

**Training details.** We trained our model on the Dense Haze [4] dataset for better performance to remove the haze of the challenge images. While we trained the model on the ITS of RESIDE [13] as a benchmark to compare our proposed method against the state-of-the-art dehazing methods. The parameter settings for the two training processes are the same as follows: Adam optimizer is adopted with a batch size of 1. The network adopts a learning rate of 0.0005. We set the exponential rates  $(\beta_1, \beta_2)$  to  $(0.6, 0.999)$ .  $(\lambda_1, \lambda_2)$  in Equation 1 is set to  $(1, 5)$  empirically. We carry out our model with PyTorch framework in 1 TITAN GPU.

**Quality measures.** As for qualitative evaluation, we measure the result of our method in terms of two evaluation metrics: the Peak Signal to Noise Ratio (PSNR) and the Structural Similarity index (SSIM), which are often used as criteria for evaluating image quality in dehazing. Furthermore, we evaluate and compare our dehazing effects with the subjective visual effects.

### 4.3. Comparisons with state-of-the-art methods

We compare the proposed method with two representative prior-based methods: Dark Channel Prior (DCP) [8], Non-local Image Dehazing (NLD) [1], and three advanced learning-based methods: ALL-in-One Dehazing Network (AOD-Net) [12], DehazeNet [2] and Gated Fusion Network (GFN) [20].

**Results on synthesis dataset.** Table 1 and Figure 4 show the quantitative and qualitative results of our method and other comparison methods on synthesis dataset. In Table 1, our method achieves the best performance on the two metrics PSNR and SSIM. Our PSNR surpasses the second place 1.72 dB in indoor testing and 1.18 dB in outdoor testing, while SSIM is 0.0421 and 0.0372 higher than the second in indoor and outdoor separately.

From Figure 4, we see that DCP [8] is not fine for the recovery of some details. Particularly for hazy images with sky region, the effect of DCP [8] is significantly reduced, which is its inherent disadvantage. NLD [1] has apparent color distortion and produces some unrealistic tones because the prior on which it is based is not robust. The result images processed by AOD-Net [12] and DehazeNet [2] still remain some noticeable hazy. GFN [20] recovers some details more clearly, however it generates some artifacts and over-saturated colors. Note that on the outdoor test set, GFN [20] failed to exhibit the desired performance. Both on the indoor and outdoor synthesis dataset, our network shows the best visual effect.

**Results on a real-world dataset.** We further evaluate the proposed model on a real-world dataset collected by previous works. A satisfactory result is that our model also shows superior performance, indicating that our model has good robustness and scalability. Shown as Figure 5, prior-based methods DCP [8], NLD [1] generate unrealistic tones

Table 2. Quantitative comparisons of different  $(\lambda_1, \lambda_2)$  on SOTS outdoor.

$(\lambda_1, \lambda_2)$	(10,1)	(5,1)	(1,1)	(1,5)	(1,10)
PSNR	20.81	19.55	19.93	23.64	22.35
SSIM	0.8728	0.8530	0.8453	0.9137	0.8859

which cause the images color-distorted. AOD-Net [12] and DehazeNet [2] still remain residual haze. GFN can not work well in dense fog areas. In comparison, our model restores images more naturally and realistically.

**Results on Dense Haze [4].** The Dense Haze [4] dataset can be a pretty challenge for dehazing task because of the heavy fog. We use the proposed model to test on both the validation and testing images. As shown in Figure 6, for the initial input filled with thick fog, although not completely removing all the haze, our method relatively shows superior effect and better restores the details and color information of the image.

**Results on I-HAZE [17] & O-HAZE [3].** In order to better present our model, we performed extensive experiments on the NTIRE2018 dehazing challenge [5] datasets (I-HAZE [17] and O-HAZE [3]). It is worth noting that we used the model trained on the RESIDE [13] to test the images from NTIRE2018 datasets and achieved promising results, which shows the robustness of our model. Figure 7 shows the visual results.

### 4.4. Ablation study

For loss function in Equation 4, different parameter settings of  $(\lambda_1, \lambda_2)$  should contribute to different performances. To examine the influence of the hyper-parameters settings and select an optimal value for training, we conduct a series of tests on  $(\lambda_1, \lambda_2)$  in SOTS outdoor. The results of average PSNR, SSIM, as well as corresponding settings are shown in Table 2. The network performs best when  $(\lambda_1, \lambda_2)$  is set to  $(1, 5)$ .

In order to intentionally analyse and demonstrate the effectiveness of the different components of the architecture, we designed the following ablation experiments: 1) w/o AD block: replace AD block with other block; 2) w/o ME module: remove the two enhancing blocks; 3) single ME: retain only one enhancing block. The results with corresponding configurations of three ablation variants are shown in Table 3 and Figure 8. We observed that the proposed structure outperforms the other variants both in the measure criteria and visual effect. As for the variant without AD, we replace the AD block with 6 regular convolutions with kernel size  $3 \times 3$ . Considering the consistency of other variables, we concatenate the input to the convolution output. Contrast with the replacement, the proposed method leads 2.49 dB in PSNR and 0.04 dB in SSIM respectively, which shows that the AD block is indeed valid. As our ME mod-

Table 1. Quantitative comparisons of the state-of-the-art dehazing methods and our method on SOTS.

Method		DCP [8]	NLD [1]	AOD-Net [12]	DehazeNet [2]	GFN [20]	Ours
indoor	PSNR	16.62	17.57	19.06	21.14	22.30	24.02
	SSIM	0.8179	0.81	0.8504	0.8472	0.8800	0.9221
outdoor	PSNR	19.13	17.97	20.29	22.46	21.55	23.64
	SSIM	0.8148	0.7791	0.8765	0.8514	0.8444	0.9137

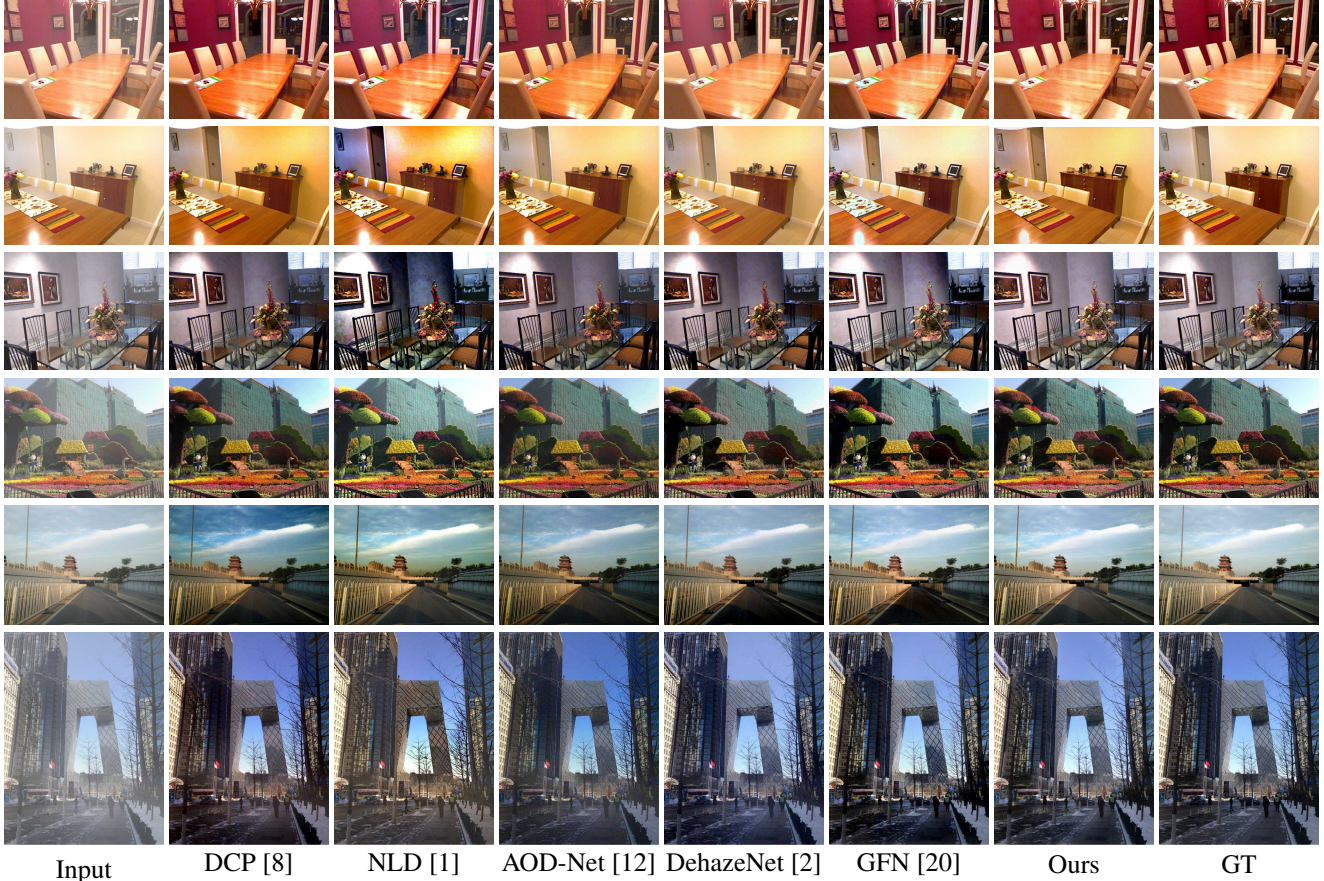


Figure 4. Qualitative result of the state-of-the-art dehazing methods and our proposal on synthetic dataset. The upper three rows are the results on SOTS-indoor images and the bottom three rows are the results on SOTS-outdoor images.

ule consists of two enhancing blocks, to better investigate the influence of the enhancing block, we implement the architectures with no and single enhancing block respectively. Comparing these three models, it can be obviously seen that the structure without ME shows the worst effect. The structure with single enhancing block performances slightly better, however it introduces some degree of color distortion. Our method is superior to single enhancement since the second enhancing block further fuses the refinements from the first and the feature maps learned by distillation. In summary, the enhancing block does works in refining features and improving performance, and two enhancing blocks remove haze more effective than one does. The above ablation

Table 3. Ablation settings and results on SOTS-outdoor.

Method	AD block	enhancing block	PSNR	SSIM
w/o AD	-	√	21.15	0.8737
w/o ME	√	-	21.94	0.8840
single ME	√	1	23.09	0.9073
Ours	√	√	23.64	0.9137

experiments demonstrate that our designed adaptive distillation block and multi-scale enhancing block are efficient.

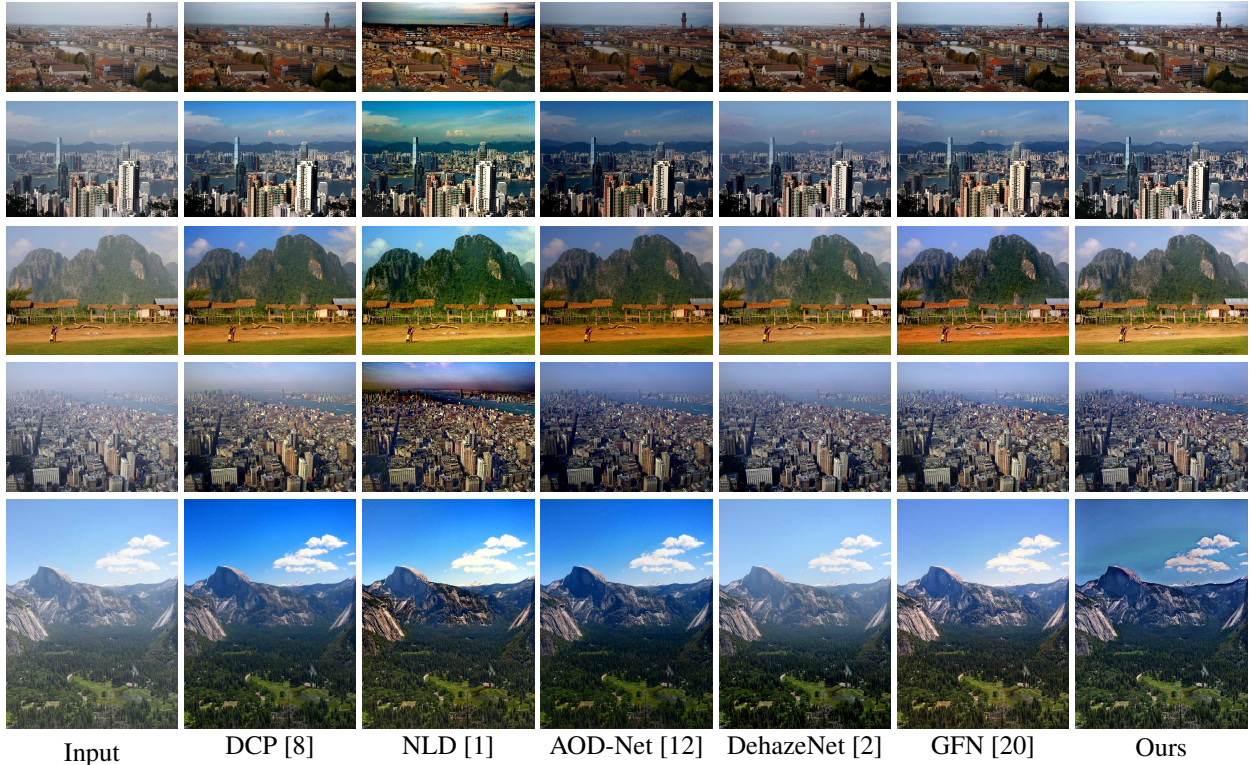


Figure 5. Qualitative result of the state-of-the-art dehazing methods and our method on the real dataset.

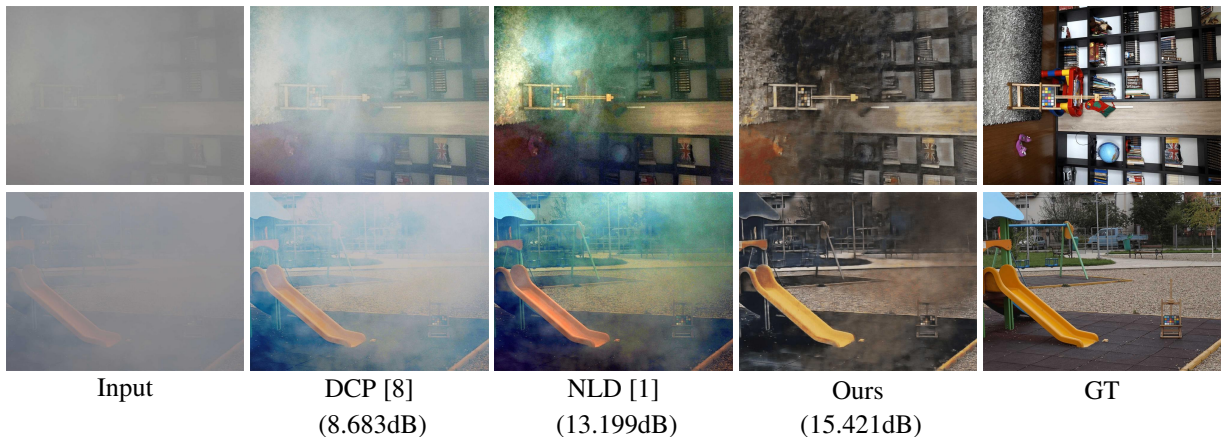


Figure 6. Visual results on Dense Haze [4]. The value below each methods denotes the corresponding average PSNR.

## 5. Conclusion

In this paper, we propose an adaptive distillation network which directly dehazes on single image independent of the atmospheric scattering model. Besides, we introduce a multi-scale enhancing module consisting of two enhancing blocks to refine the distillation results. To optimize the quality of hazy-free image, we combine the perceptual loss with the similarity loss. We implement our model on various datasets involving indoor and outdoor. Comparing with

other representative dehazing methods, our results achieve satisfactory PSNR and SSIM values as well as visual effect. Moreover, we perform additional ablation experiments to demonstrate the effectiveness of the various compositions of the network.

## 6. Acknowledgements

This work was supported by the National Natural Science Foundation of China under Grant 61876161, and Grant U1065252.

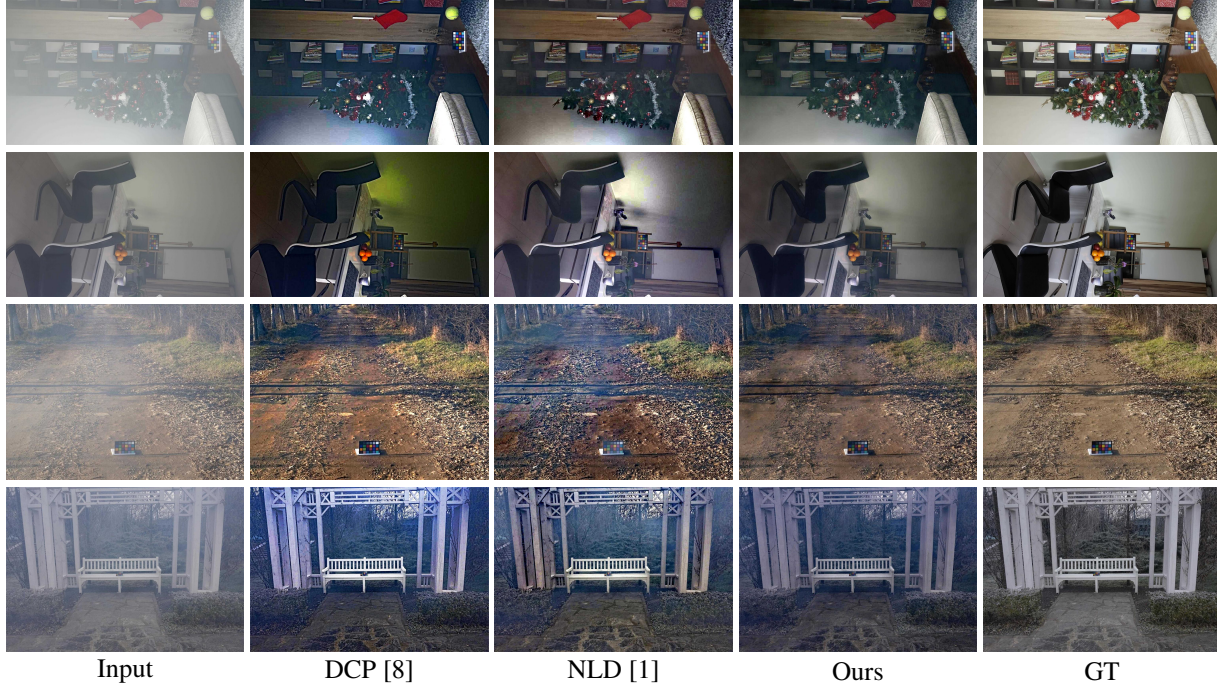


Figure 7. Qualitative results on NTIRE2018 challenge datasets. The upper two rows show the dehazing results on I-HAZE [17] and the bottom two rows show the dehazing results on O-HAZE [3].

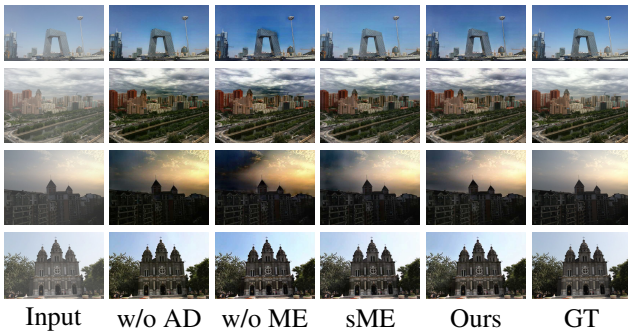


Figure 8. Qualitative result of ablation study on SOTS-outdoor.

## References

- [1] Dana Berman, Shai Avidan, et al. Non-local image dehazing. In *Proceedings of the IEEE conference on computer vision and pattern recognition*, pages 1674–1682, 2016.
- [2] Bolun Cai, Xiangmin Xu, Kui Jia, Chunmei Qing, and Dacheng Tao. Dehazenet: An end-to-end system for single image haze removal. *IEEE Transactions on Image Processing*, 25(11):5187–5198, 2016.
- [3] Christophe De Vleeschouwer Radu Timofte Codruta O. Ancuti, Cosmin Ancuti. O-haze: a dehazing benchmark with real hazy and haze-free outdoor images. *2018 NTIRE, IEEE Conference on Computer Vision and Pattern Recognition Workshops (CVPRW), Salt Lake City, US 2018*.
- [4] Mateu Sbert Radu Timofte Codruta O. Ancuti, Cosmin Ancuti. Dense haze: A benchmark for image dehazing with dense-haze and haze-free images. *arXiv:1904.02904*, 2019, 2019.
- [5] Radu Timofte et al Cosmin Ancuti, Codruta O. Ancuti. Ntire 2018 challenge on image dehazing: Methods and results. *2018 NTIRE, IEEE Conference on Computer Vision and Pattern Recognition Workshops (CVPRW), Salt Lake City, US 2018*.
- [6] Raanan Fattal. Dehazing using color-lines. *ACM transactions on graphics (TOG)*, 34(1):13, 2014.
- [7] Ian Goodfellow. Nips 2016 tutorial: Generative adversarial networks. *arXiv preprint arXiv:1701.00160*, 2016.
- [8] Kaiming He, Jian Sun, and Xiaoou Tang. Single image haze removal using dark channel prior. *IEEE transactions on pattern analysis and machine intelligence*, 33(12):2341–2353, 2011.
- [9] Jie Hu, Li Shen, and Gang Sun. Squeeze-and-excitation networks. In *Proceedings of the IEEE conference on computer vision and pattern recognition*, pages 7132–7141, 2018.
- [10] Zheng Hui, Xiumei Wang, and Xinbo Gao. Fast and accurate single image super-resolution via information distillation network. In *Proceedings of the IEEE Conference on Computer Vision and Pattern Recognition*, pages 723–731, 2018.
- [11] Justin Johnson, Alexandre Alahi, and Li Fei-Fei. Perceptual losses for real-time style transfer and super-resolution. In *European conference on computer vision*, pages 694–711. Springer, 2016.
- [12] Boyi Li, Xiulian Peng, Zhangyang Wang, Jizheng Xu, and Dan Feng. Aod-net: All-in-one dehazing network. In *Proceedings of the IEEE International Conference on Computer Vision*, pages 4770–4778, 2017.

- [13] Boyi Li, Wenqi Ren, Dengpan Fu, Dacheng Tao, Dan Feng, Wenjun Zeng, and Zhangyang Wang. Benchmarking single-image dehazing and beyond. *IEEE Transactions on Image Processing*, 28(1):492–505, 2019.
- [14] Youssef Alami Mejjati, Christian Richardt, James Tompkin, Darren Cosker, and Kwang In Kim. Unsupervised attention-guided image-to-image translation. In *Advances in Neural Information Processing Systems*, pages 3693–3703, 2018.
- [15] W. E. K. Middleton. Vision through the atmosphere. *Physics Today*, 7(3):21–21, 1954.
- [16] Bharath Raj N. and . Venkateswaran, N. Single image haze removal using a generative adversarial network. 2018.
- [17] Christophe De Vleeschouwer Radu Timofte odruta O. Ancuti, Cosmin Ancuti. I-haze: a dehazing benchmark with real hazy and haze-free indoor images. *International Conference on Advanced Concepts for Intelligent Vision Systems, LNCS, Springer, Poitiers, France, 24-27 Sept 2018*.
- [18] Ido Omer and Michael Werman. Color lines: Image specific color representation. In *Proceedings of the 2004 IEEE Computer Society Conference on Computer Vision and Pattern Recognition, 2004. CVPR 2004.*, volume 2, pages II–II. IEEE, 2004.
- [19] Wenqi Ren, Si Liu, Hua Zhang, Jinshan Pan, Xiaochun Cao, and Ming-Hsuan Yang. Single image dehazing via multi-scale convolutional neural networks. In *European conference on computer vision*, pages 154–169. Springer, 2016.
- [20] Wenqi Ren, Lin Ma, Jiawei Zhang, Jinshan Pan, Xiaochun Cao, Wei Liu, and Ming-Hsuan Yang. Gated fusion network for single image dehazing. In *Proceedings of the IEEE Conference on Computer Vision and Pattern Recognition*, pages 3253–3261, 2018.
- [21] Xitong Yang, Zheng Xu, and Jiebo Luo. Towards perceptual image dehazing by physics-based disentanglement and adversarial training. In *Thirty-second AAAI conference on artificial intelligence*, 2018.
- [22] Hongyuan Zhu, Xi Peng, Vijay Chandrasekhar, Liyuan Li, and Joo-Hwee Lim. Dehazegan: When image dehazing meets differential programming. In *IJCAI*, pages 1234–1240, 2018.
- [23] Qingsong Zhu, Jiaming Mai, and Ling Shao. A fast single image haze removal algorithm using color attenuation prior. *IEEE transactions on image processing*, 24(11):3522–3533, 2015.